A Lightweight Robotic Leg Prosthesis Replicating the Biomechanics of the Knee, Ankle, and Toe Joint

Minh Tran[1,*], **Lukas Gabert**[1,*], **Sarah Hood**[1], **Tommaso Lenzi**[1,†]

[1]Department of Mechanical Engineering and Robotics Center, University of Utah, Salt Lake City, UT, USA

Abstract

Robotic leg prostheses promise to improve the mobility and quality of life of millions of individuals with lower-limb amputations by imitating the biomechanics of the missing biological leg. Unfortunately, existing powered prostheses are much heavier, bigger, and have shorter battery life than conventional passive prostheses, severely limiting their clinical viability and utility in the daily life of amputees. Here, we present a robotic leg prosthesis that replicates the key biomechanical functions of the biological knee, ankle, and toe in the sagittal plane while matching the weight, size, and battery life of conventional microprocessor-controlled prostheses. The powered knee joint uses a unique torque-sensitive mechanism combining the benefits of elastic actuators with that of variable transmissions. A single actuator powers the ankle and toe joints through a compliant underactuated mechanism. Since the biological toe dissipates energy while the biological ankle injects energy into the gait cycle, this underactuated system regenerates substantial mechanical energy and replicates the key biomechanical functions of the ankle/foot complex during walking. A compact prosthesis frame encloses all mechanical and electrical components for increased robustness and efficiency. Preclinical tests with three individuals with above-knee amputation show that the proposed robotic leg prosthesis allows for common ambulation activities with close to normative kinematics and kinetics. Using an optional passive mode, users can walk on level ground indefinitely without charging the battery, which has not been shown with any other powered or microprocessor-controlled prostheses. A prosthesis with these characteristics has the potential to improve real-world mobility in individuals with above-knee amputation.

Summary

A powered prosthetic leg that replicates key biomechanics and matches the weight, size, and battery life of passive devices.

Introduction

To date, most prostheses available to individuals with above-knee amputation are passive devices that cannot replicate key biomechanical functions of the missing biological leg. Most ankle/foot prostheses consist of a carbon fiber plate enclosed in a rubber foot shell (1). Some ankle-foot prostheses have an actual ankle joint actuated by passive elements such as springs and dampers. Virtually all available ankle/foot prostheses rely on the flexibility of the rubber foot shell to emulate the movement of the metatarsal joint (toe joint) and only one ankle-foot prosthesis available on the market has an articulated, passive toe joint (2). For above-knee patients, the ankle/foot prosthesis is connected to a prosthetic knee, which may have a single-joint or polycentric design, passively actuated by springs and dampers (3). In microprocessor-controlled prostheses, the mechanical impedance of the ankle and knee joint can be actively adjusted during gait to facilitate walking at a variable cadence while improving stability and reducing the risk of falls (4). However, they cannot actively generate movements or inject net-positive energy into the gait cycle (5), which are key biomechanical functions of biological legs (6, 7). Prosthesis users compensate for these deficiencies with their residual limb and contralateral leg resulting in a slower, less efficient, and less stable gait compared to nonamputees (8). Since these passive prostheses cannot actively generate knee torque, climbing stairs and ramps or transitioning between sitting and standing is much more challenging for individuals with above-knee amputations than nonamputees. As a result, most individuals with an above-knee amputation are not able to ambulate in the community (8). Improvements in prosthetic technologies are necessary to address the unmet needs of the millions of individuals living with lower-limb amputation (9).

Robotic leg prostheses promise to improve the ambulation ability of individuals with lower-limb amputation by imitating key biomechanical functions of the missing biological leg with onboard actuation systems, sensors, and power supplies (10). Researchers have proposed different advanced actuation designs to efficiently provide the wide ranges of speed and torques needed to imitate the biological leg (6, 7). Powered knee prostheses can be actuated using springs in series (11) and parallel to a motor (12), multi-joint actuators (13), antagonistic actuators (14), or high-torque density motors (15). Similarly, powered ankle prostheses can be actuated using four-bar mechanisms and polycentric designs (16–18), using a spring in parallel or in series to the motor (19), inductive charging (20), or implementing clutches and brakes in combination with motors (21, 22). These advanced actuation systems have enabled two powered prostheses to reach the market. The Ottobock Empower ankle/foot prosthesis uses a series/parallel elastic actuator (23), whereas the Ossur Power Knee uses a clutchable series-elastic actuator (24). Unfortunately, after several years on the market, powered prostheses have failed to achieve clinical success (25–28). Although this negative outcome likely results from a combination of factors, there are key design limitations that affect function and usability of existing powered prostheses. These powered devices are much heavier, bigger, and have shorter battery life than their passive counterparts. Increasing the prosthesis weight affects both biomechanics and clinical outcomes negatively. During walking, larger prosthesis weight has been correlated to increased metabolic energy cost (29), stance-time and swing-time asymmetries (30) hip effort (31), and reduced socket stability. Increasing the prosthesis build height and the

distance between the knee center of rotation and the top of the pyramid has limited the number of people that can be fitted to the prosthesis. Moreover, powered prostheses have much shorter battery life than their passive counterparts—a few hours versus a few days—which has a negative effect on usability in real life. We need to decrease the weight and size and extend the battery life of robotic leg prostheses to improve their clinical effect.

An alternative design strategy for robotic leg prostheses consists of powering only a subset of activities (32–35), avoiding net-positive energy injection, or adjusting the mechanical behavior of the prosthetic joint without actively controlling movements or injecting energy(36–39). By relaxing the actuation speed and torque requirements, these semi-active and quasi-passive prostheses can be made lighter, smaller, and still achieve longer battery life than fully powered prostheses. For example, designing the knee actuator to power only stair ambulation (33, 34) or only the swing phase of gait (32, 40) leads to a lighter and smaller prosthesis. Similarly, lighter and smaller ankle/foot prostheses can be developed by avoiding net-positive energy injection (41), limiting the active control of movements to non-weight bearing activities (38, 42), or to adjusting the mechanical stiffness of the prosthetic joint (37). More recently, switching gears between different ambulation activities has been proposed to bridge the gap between semi-active and fully powered prostheses. However, this design solution comes at the cost of functionality, as the prosthesis cannot provide torque while switching gears(43–45). Thus, semi-active and quasi-passive prostheses are typically lighter, smaller, and have longer battery life than fully powered devices but cannot replicate key biomechanical functions of the missing biological leg.

Biomechanical studies of nonamputee gait suggest that the metatarsal (toe) joint plays an important function during gait (46). Individuals with metatarsophalangeal arthrodesis (fusion of the toe joint) have decreased step length and reduced plantarflexion moment in the affected side(47). Studies with a passive prosthesis emulator show that the stiffness of the toe joint has a substantial effect on ankle power, center of mass, and push-off work during walking(48). Moreover, a previous study has shown improvements in the metabolic cost of walking of individuals with below-knee amputations using a passive prosthesis with midfoot and metatarsophalangeal joints (49). Despite this evidence, only one research robotic ankle/foot prosthesis has been designed with a powered toe joint (50, 51). Unfortunately, the added toe function comes at the cost of a substantial increase in prosthesis weight due to the addition of a dedicated toe actuator. Thus, we need new designs that can replicate the biomechanical function of the toe joint in a lightweight prosthesis.

Here we present a robotic leg prosthesis designed to replicate the key biomechanical functions of the biological knee, ankle, and toe joints in the sagittal plane while matching the weight, size, and battery life of microprocessor-controlled prostheses. As we will show, this level of lightness, performance, and efficiency is enabled by bioinspired actuation designs combined with a holistic design approach(52). Using biomechanical analysis, analytical models, and dynamic simulations, we will show that a unique torque-sensitive actuator can replicate key biomechanical features of the biological knee joint by combining the benefits of series elastic actuators with that of variable transmissions. We will also show that an actuator based on a compliant underactuated mechanism can replicate the ankle and toe joint functions while regenerating substantial mechanical energy during walking. Finally, we

will also show the ability to walk on level ground indefinitely without charging the battery. A prosthesis with these characteristics has the potential to improve real-world mobility in individuals with above-knee amputations.

Results

System Overview

The proposed powered prosthesis—namely Utah Bionic Leg—consists of independent knee and ankle/foot modules (Figure 1.A). The knee module uses a unique torque-sensitive actuator that works as a variable transmission to change the torque ratio passively, continuously, and quickly in response to varying knee extension torque by following a specific curve defined by the design geometry. The ankle/foot module uses a compliant, underactuated mechanism to power both the ankle and the toe joint. This compliant, underactuated mechanism transfers mechanical energy from the toe to the ankle joint, improving efficiency, while storing and releasing energy in a lightweight spring assembly. The knee and the ankle/foot modules have independent onboard power supplies and embedded electronic systems (Figure 1.B). Both modules are designed based on ISO standards, facilitating their use outside the laboratory. The powered knee module of the Utah Bionic Leg has similar weight and size to the Ottobock C-leg—a microprocessor-controlled knee prosthesis (53). The powered ankle/foot module has similar weight and size to the Ottobock Meridium—a microprocessor-controlled ankle/foot prosthesis (54). Our powered knee module is slightly lighter (40 g, 2.3%) and has a shorter pyramid-to-knee joint length than the C-Leg Genium (3 mm, 11.5%). Our ankle module is slightly taller (4 mm, 5%) and heavier (70 g, 4%) than the Ottobock Meridium, although our powered device includes a custom force/torque sensor (55), which is not present in the Meridium. Most importantly, our powered knee and ankle/foot prosthesis is substantially smaller and lighter than the Ossur POWER KNEE™ (24) and the Ottobock Empower™ (23) —the only powered devices on the market. Similarly, powered prostheses designed by research laboratories that have not yet been marketed are between ~50% and ~100% heavier than the Utah Bionic Leg, which has an additional powered toe joint and embeds all the mechanical and electrical components (11, 56–58). Both commercially-available and research powered prostheses have a larger joint axis to pyramid length compared to the Utah Bionic Leg. Although battery life depends on many factors, the Utah Bionic Leg can be operated in passive mode, enabling the user to walk without needing to charge the battery. In this passive mode, the knee joint behaves primarily as a damper whereas the ankle joint behaves primarily as a spring, and they imitate the mechanical behavior of microprocessor-controlled knee and ankle/foot prosthesis. This functionality has never been shown by any existing powered or microprocessor-controlled prostheses.

Analysis of the Torque-Sensitive Knee Actuator

Our torque-sensitive actuator is inspired by the biomechanical analysis of the biological knee joint. This analysis shows that the knee generates almost four times the torque in extension than flexion (1.21 vs. 0.3 Nm/kg) and the peak extension torque is more than double in stair ascent compared to level-ground walking (1.21 vs. 0.51 Nm/kg). In contrast, the knee extension velocity is three times higher during walking than stair ascent (339 vs. 99

°/s), although the peaks of the knee flexion velocity are similar between the two activities. The stance phase (foot on the ground) requires much greater torque and lower velocity than the swing phase (foot off the ground) for both level-ground walking and stair ascent (Figure 2.A). Thus, the biological knee joint produces wide ranges of torques and speeds during ambulation, but the peak of knee torque and speed are not simultaneous. Providing wide ranges of torques and speeds with a small and lightweight electrical actuator is challenging because mechanical power output and electrical efficiency decrease sharply outside narrow ranges of torque and speed (59, 60). Our torque-sensitive actuator aims to address this issue by altering the torque ratio in response to knee extension torque.

Dynamic simulations show how the passively variable torque ratio affects the motor speed/ torque requirements by comparing the performance of a torque-sensitive actuator to that of the same actuator fixed at the maximum or minimum of the torque ratio range (Figure 2.B). These simulations suggest that using the actuator at a fixed high-torque ratio would not satisfy the winding voltage limit, primarily due to the high velocity required in the swing phase (Figure 2.C). Moreover, the simulations show that using the actuator at a fixed low-torque ratio would exceed the maximum current limit during stair ascent, primarily due to the high torque required in stance (Figure 2.C). In contrast, the torque-sensitive actuator can satisfy both motor torque and speed requirements by adapting the torque ratio during ambulation. In stance, when the knee torque is high and the speed is low, the torque ratio quickly increases from its minimum to its maximum, lowering the required motor torque for both walking and stair ascent (Figure 2.B). In the swing phase, when the knee torque is low and the speed is high, the torque ratio stays close to its minimum, reducing the required motor speed as well as the inertial torque (Figure 2.B). Because the knee speed is low when the torque is high (Figure 2.A), increasing the torque ratio proportionally to the knee extension torque does not cause the motor to reach the winding limit even though the motor velocity is higher than it would be without the torque-sensitive actuator during stance (Figure S4). Thus, the simulations show that by leveraging the non-simultaneous peaks of torque and speed, the torque-sensitive actuator can reduce the motor speed/torque requirements, enabling a small, lightweight motor to efficiently provide the wide ranges of torques and speeds required for a knee prosthesis.

Analysis of the Compliant, Underactuated Ankle-Toe Mechanism

Our compliant, underactuated mechanism is inspired by the biomechanical analysis of the biological ankle/foot complex. This analysis (Figure 2.D) shows that during walking, the toe torque is nearly proportional to the ankle torque for a large part of the stance phase (20–60% Stride), although the peak torque is much lower for the toe than the ankle (0.12 Nm/kg versus 1.35 Nm/kg). Moreover, the velocities of the two joints are comparable in magnitude and opposite in direction, peaking at −218 °/s and 280 °/s for the ankle and toe joint, respectively. As a result, the toe dissipates power whereas the ankle generates power. Thus, during walking, the ankle and toe torque are nearly proportional, and the combined ankle and toe power is smaller than the power of the ankle alone. This analysis suggests that a single actuator could power both the ankle and toe joint, requiring fewer mechanical and electrical components than using two separate actuators. Moreover, this analysis shows that the combined ankle and toe power is smaller than the power of the ankle alone. Powering

both the ankle and toe joints in a prosthesis is challenging due to the stringent weight and size requirements. Our compliant, underactuated mechanism aims to address this issue by enabling a single actuator to efficiently power both the ankle and the toe joints.

Dynamic simulations show the function of the compliant, underactuated system during walking by comparing its performance to that of an equivalent actuator powering the ankle joint only. The energy flow analysis (Figure 2.E) shows that, the ankle-only design requires 14.4 J/stride of electrical energy to produce 6.3 J/stride of mechanical energy at the ankle, achieving an overall efficiency of 43.8%. In comparison, the underactuated design requires 8.2 J/stride of electrical energy, achieving an overall efficiency of 76.8%. Thus, the electrical energy consumption per stride is 43.0% lower in the underactuated design (Figure 2.F). The energy flow analysis also shows that the reduced electrical energy consumption is primarily due to the toe regenerating 4.5 J/stride of mechanical energy. Finally, the underactuated system shows lower energy losses than the ankle-only design (−1 J/stride of Joule heating and −0.5 J/stride of friction). These lower energy losses are due to the lower velocity and acceleration of the linear actuator in the underactuated design, which result in lower inertial torque and mechanical power output at the motor (Figure 2.E). Thus, the simulations show that by leveraging the concurrent torque generation at the biological toe and ankle joints, a compliant underactuated design can enable a single actuator to power both the ankle and toe joint and also reduce electrical energy consumption.

Performance Verification of the Powered Knee and Ankle/foot Modules on the Bench

The knee closed-loop step position tests (Figure 3.A) showed rise times between 37 ms and 56 ms, depending on the position step size. Thus, the −3 dB bandwidth of the knee position controller was between 9.5 Hz and 6.2 Hz, which exceeded the position bandwidth of the biological knee (61). Output impedance tests showed that the minimum-backdriving torque measured by the external 6-axis load cell with the motors off was 0.3 Nm (Figure 3.B), which was lower than other powered knee prostheses (3.2 Nm (58), 2.6 Nm (62), 3–5 Nm (56)). Based on system identification of the output impedance (Figure 3.B), the damping and inertia at the output joint were 0.43 Nms/rad and 0.04 kgm^2, respectively. The low minimum backdriving torque and output impedance of the knee module was essential to allow for passive swing motion (Video S3). Also, based on the reading of an external 6-axis load cell, the knee torque step response showed steady-state errors lower than 1.2% and a rise time of ~32 ms irrespective of torque direction, resulting in a −3 dB bandwidth of ~11 Hz (Figure 3.C), which was greater than that of the biological knee (61). Since the torque-sensitive joint acted in extension only, and the torque step response was nearly identical in extension and flexion, we conclude that the torque-sensitive joint did not affect the bandwidth of the open-loop torque controller (Figure 3.C). The motor current during the torque step response test was 18–26% lower in extension than in flexion, because the torque-sensitive joint only changed the torque ratio in response to extension torque (Figure 3.C). The continuous motor current increased from 4.21 A (the rated value) to 9.91 A (a 135% increase), as the contact between the motor and the frame provided enhanced thermal dissipation (35) (Figure 3.D). This enhanced thermal dissipation was critical for the powered knee module to provide biomechanically appropriate function without overheating (see Supplementary Methods). Locking the torque-sensitive joint removed the ability of the

knee module to increase the torque ratio (Figure 3.E). With the torque sensitive joint locked at the bottom end, the Joule heating losses increased by 140%, so the knee could not provide more than 90 Nm without overheating. This torque level was 40% lower than the 150 Nm limit with the torque-sensitive unlocked and is not sufficient for most people in the United States (75 percentile adult male and 46 percent female) (63) to naturally climb stairs or stand up from a seated position. Locking the torque-sensitive joint at the top end can address this torque limitation. However, it lowered the maximum knee joint velocity substantially due to voltage saturation at the motor, and the knee module could not perform natural swing phase movements in waking and stair ascent (Figure 3.F), which may cause the user to scuff, stumble, and fall. Thus, the torque-sensitive joint was essential for the knee module to satisfy basic torque and speed requirements for ambulation.

The ankle closed-loop step position tests (Figure 4.A) showed rise times between 30 ms and 61 ms, resulting in −3 dB bandwidths between 12 Hz and 6 Hz. The sine-wave position test of the underactuated ankle mechanism showed that if the toe joint moves in phase with the ankle joint the peak velocity of the linear actuator reduced from ~25 mm/s to 1 mm/s, a 95% decrease (Figure 4.B). Thus, the underactuated mechanism could substantially reduce the required motor speed when the toe and ankle joint moved in phase. The ankle torque step response (Figure 4.C) showed rise times between 32 ms and 25 ms, depending on the torque direction. These differences were consistent with the measured stiffness of the series spring (Figure 4.D) in tension (829 N/mm) and compression (1273 N/mm). For the tested conditions, the bandwidth of the ankle torque controller was between 14 Hz and 11 Hz, which exceed the torque generation bandwidth of the biological knee and ankle (61). The continuous current increased from 7.58 A (the rated value) to 10.30 A, a 36% increase (Figure 4.E), as the motor was in contact with the frame. Thus, the thermal dissipation was necessary for the ankle module to provide biomechanically appropriate function without overheating (see Supplementary Methods). Output impedance tests (Figure 4.F) with an external 6-axis load cell showed that the minimum-backdriving torque with the motors off was 1.2 Nm, which was about half of other powered prostheses tested under similar conditions (3.2 Nm (58), 3–5 Nm (56)). System identification estimated the damping and inertia at the output joint to be 2.18 Nms/rad and 0.35 kgm^2, respectively.

Validation of the Powered Knee-Ankle-Toe Prosthesis During Common Ambulation Tasks

Clinically relevant ambulation goals derived from nonamputee biomechanics (64–67) provided a reference to assess the performance of the Utah Bionic Leg during ambulation with three above-knee amputee participants (Figure 5). Table 1 provides an in-depth assessment of the performance and main results are summarized hereafter.

During walking in standard mode, the knee joint was slightly flexed at heel strike (9.3±3.1°, mean ± S.D.) and stance knee flexion peaked at 13.7±5.0°. However, there were substantial differences between participants. For Participants 1 and 3, the stance knee flexion was minimal. So, the knee extension torque was generally low, and the torque-sensitive joint stayed close to its minimum. In contrast, Participant 2 showed physiological stance knee flexion and knee extension torque. The torque-sensitive joint extended as expected from simulations, causing the knee torque ratio to increase proportionally. Also, in standard

mode, the ankle plantarflexion torque at push-off reached 1.50±0.10 Nm/kg, which was within 2% of normative value and within 5% of normative timing. The maximum angle and torque of the toe joint were 36.3±1.1° and 0.12±0.02 Nm/kg, respectively, which were close to biomechanical goals of 39.6° and 0.12 Nm/kg. In the swing phase, both the knee and the ankle joint trajectory closely followed the normative data. Walking in standard mode with the toe joint locked had a visible effect on the ankle kinetics and kinematics (Figure S10). The peak motor velocity increased by 47%, resulting in a 56% increase in the peak motor mechanical power. Due to the motor approaching the winding limitation, the ankle mechanical energy decreased by ~18%, from 0.17 J/kg with the toe unlocked to 0.14 J/kg with the toe locked. Despite the lower ankle mechanical energy, the electrical energy consumption increased by 24% with the toe locked. In passive mode, there was no active ankle push-off or visible stance knee flexion, similar to a passive prosthesis. Both the maximum ankle plantarflexion torque and dorsiflexion angle of the ankle were within 10.0% of the passive prosthesis reference. In the swing phase, the ankle angle is near 0°, and little active dorsiflexion movement is shown. Also, in the swing phase, the knee achieved 63.8±1.3° showing an extension timing within 0.7±0.2% of passive prosthesis reference, which allowed for proper foot clearance. Thus, the Utah Bionic Leg enabled the amputee participants to walk safely both in standard and passive mode, even though the standard mode better satisfied the clinically relevant ambulation goals. Moreover, locking the toe reduced electrical efficiency and mechanical power output of the ankle module.

When climbing stairs one step at a time (Figure 6), the powered knee generated biomechanically accurate torque, peaking at 1.08±0.08 Nm/kg, within 1.4±1.4% of able-bodied timing. However, the prosthetic knee joint extended faster than the biological knee, which resulted in a peak mechanical power 28.5% higher than the physiological value (3.25±0.19 W/kg). In contrast, the maximum ankle plantarflexion torque (0.62±0.07 Nm/kg) was considerably lower than the normative value (1.27 Nm/kg). When climbing stairs two steps at a time, the knee provided up to 1.67±0.13 Nm/kg of extension torque and 4.71±0.36 W/kg of positive mechanical power, which corresponded to a 54.6% and 44.9% increase, respectively, compared to climbing stairs one step at a time. In the swing phase, the knee and the ankle module closely followed the able-bodied reference (Table 1), safely clearing the step and positioning the prosthetic foot in preparation for the next step to be taken. In the stance phase, the knee torque ratio increased proportionally to the knee extension torque until it reached its maximum for all stair climbing conditions. In the swing phase, the knee extension torque is low, so the torque ratio stayed close to its minimum (Figure 6). Thus, the Utah Bionic Leg provided appropriate torque, clearance, and foot placement to enable climbing stairs both one and two steps at a time, which was not possible with microprocessor-controlled prostheses.

In stair descent, the powered knee generated up to 1.05±0.12 Nm/kg of extension torque, which was within 25% of nonamputee data (1.34 Nm/kg). The ankle dorsiflexed up to 19.3±0.7°, slowing down the stair descent movement. Also, the toe showed a peak extension of 36.0±1.0°, enabling the prosthesis to maintain stable contact with the step. In the swing phase, the prosthetic knee flexed to safely clear the step, with timing similar to able-bodied data (1.5±1.7%). Also, in the swing phase, the ankle plantarflexed up to 9.9±0.2°, enabling the foot to contact the subsequent step with the toe first. Consistently with the controller

in use (68), there were visible differences between the ankle kinetics and the nonamputee reference. Similar to stair ascent, the knee torque ratio reached its maximum during stance when the knee extension torque was high and it stayed close to its minimum in swing (Figure 6). The Utah Bionic Leg provided sufficient torque and range of motion to enable descending stairs while placing the whole foot on the step.

Actuation Performance and Battery Life

The actuation performance during ambulation was assessed by estimating mechanical and electrical energy consumption based on the actuator models and the embedded sensors (see Supplementary Methods). These estimates showed that, when walking in standard mode, the knee joint absorbed 0.27±0.04 J/kg of mechanical energy per stride, while the ankle joint generated 0.23±0.03 J/kg and the toe absorbed 0.04±0.01 J/kg. After accounting for Joule heating and friction losses (Supplementary Table S6), the knee motor was estimated to regenerate 0.03±0.06 J/kg of electrical energy, whereas the ankle/toe motor was estimated to consume 0.35±0.05 J/kg of electrical energy. Thus, the total electrical energy consumption estimate in standard mode was 0.32±0.03 J/kg per stride. When walking in passive mode, the knee, ankle, and toe joints absorbed 0.15±0.01 J/kg, 0.03±0.02 J/kg, and 0.03±0.01 J/kg, respectively, of mechanical energy per stride. After accounting for Joule heating and friction losses (Table S6), the knee motor was estimated to regenerate 0.11±0.01 J/kg of electrical energy, and the ankle/toe motor was estimated to expend 0.04±0.01 J/kg of electrical energy per stride. Thus, the combined knee and ankle/foot prosthesis was estimated to regenerate 0.07±0.02 J/kg of electrical energy per stride.

Based on these estimates and accounting for the ~2 W electrical power consumption of the embedded electronic system, in standard mode, the proposed powered prosthesis would provide up to 7,730±905 strides and 15,460 steps with the current battery (2400 mAh). This battery life exceeded the 10,000 (69) and 1,500 (70)steps that nonamputee and amputee participants, respectively, take on average in a day. Moreover, in passive mode, the battery was estimated to recharge at the rate of 2.0±0.6 J per stride. Additional experiments with a single amputee participant confirmed the estimates of electrical energy by directly measuring the battery voltage and current in standard and passive mode (Figure S11). Specifically, the electrical energy consumption directly measured at the battery was 0.27 J/kg per stride in standard mode, 22% smaller than the estimated 0.35 J/kg value. In passive mode, the electrical energy regeneration measured at the battery was 0.1 J/kg per stride (Figure S12). As expected, the battery voltage decreased in standard mode and increased in passive mode (Figure S13). Thus, the Utah Bionic Leg could regenerate electrical energy during walking while providing similar kinematics and kinetics to a microprocessor-controlled prosthesis. This function could enable prosthesis users to walk on level ground indefinitely without needing to charge the battery.

Based on modeling, in step-over-step and double stair ascent, the knee motor injected 0.49±0.01 J/kg and 1.28±0.09 J/kg of mechanical energy per stride, respectively. Subtracting the energy losses due to Joule heating and friction, the knee motor required 0.89±0.10 J/kg and 2.52±0.29 J/kg of electrical energy to climb one and two steps at the time, respectively. In contrast, the ankle motor regenerated small amounts of electrical energy (Table S6).

Thus, the combined knee and ankle/foot prosthesis requires 0.88±0.17 and 2.55±0.29 J/kg of electrical energy per stride for stair ascent and double stair ascent, respectively. In stair descent, the knee motor absorbed 1.06±0.05 J/kg of mechanical energy per stride, regenerating 0.17±0.20 J/kg of electrical energy. The ankle motor absorbed 0.12±0.09 J/kg of mechanical energy per stride and regenerated 0.07±0.05 J/kg of energy. Thus, in stair descent, the combined knee and ankle/foot prosthesis regenerated 0.24±0.17 J/kg of electrical energy per stride.

Discussion

Providing wide ranges of torque and speed is necessary for powered knee prostheses to replicate the biological knee biomechanics during ambulation (Figure 2.A). Satisfying these requirements with a lightweight and compact actuator is challenging because efficiency and mechanical power output of electrical motors decrease sharply outside of a small operating range. Our analytical models show that a torque-sensitive actuator can address this problem by working like a passive variable transmission (see Supplementary Methods). Bench-top experiments confirm the model predictions by showing that when increasing the torque ratio proportionally to the knee extension torque, the required motor torque and current were substantially reduced (Figure 3.C). Notably, the motor torque decreased proportionally to the torque ratio, but the Joule heating losses decreased quadratically (Figure 3.E), which enabled a small motor (22-mm diameter, 170 g) to efficiently provide large torque at the knee joint. Although the required motor speed tends to increase as the motor torque decreases (Figure S4), the winding voltage limit is not violated because, during ambulation, the knee velocity is generally low when the knee torque is high (Figure 2.A). The torque-sensitive actuator can generate physiological swing trajectories, which was not possible when the torque-sensitive joint was locked at the top end (Figure 3.F). Thus, without the torque-sensitive joint, amputee users would not be able to safely ambulate with the proposed knee (Figure 3).The knee torque bandwidth measured experimentally was the same in flexion (non-sensitive to torque) and extension (sensitive to torque) (Figure 3.C), confirming that, different from series-elastic actuators (71), the compliance of the torque-sensitive actuator did not have a negative effect on the torque-control bandwidth. By combining a small, lightweight motor (22-mm diameter, 170 g) with a relatively low transmission ratio, the torque-sensitive actuator achieved low backdriving torque (0.3 Nm) and reflected inertia (0.04 kg m^2) (Figure 3.B). The low output impedance of the knee joint was essential for achieving electrical energy regeneration in walking. Notably, these performance improvements were obtained with a small and lightweight mechanism (~40 g) that fits into an extremely compact knee prosthesis (70 mm max width, 255 mm build height, 23 mm joint-pyramid distance, Figure 1). Thus, this study showed that the proposed torque-sensitive actuator was key to enabling lightweight and efficient knee prostheses to replicate key biomechanical functions of the biological knee joint during ambulation.

An articulated toe joint is necessary for a powered prosthesis to replicate key biomechanical functions of the missing biological foot (46, 47). However, adding a dedicated actuator for the toe joint inevitably increases the overall prosthesis weight, which has well-known negative effects on gait (72). Our experiments showed that powering the ankle and the toe joint with a single actuator could provide close to normative toe and ankle biomechanics in

walking. Not surprisingly, using a single actuator results in a lighter and smaller design compared to using two actuators (51). More importantly, experiments showed that an underactuated design could be highly efficient because substantial mechanical energy was transferred from the toe joint to the ankle joint during ambulation (~3.3 J/stride, Table S6). In accordance with the simulations (Figure 2), experiments with one amputee participant showed that locking the toe joint resulted in a substantial increase in the required motor velocity (Figure S10) and mechanical power, and consequently higher electrical energy consumption. Moreover, the mechanical energy at the ankle joint decreased, likely due to the motor reaching the winding limit. Thus, locking the joint had a substantial negative effect on the performance of the proposed ankle/foot prosthesis by spending more electrical energy to generate less mechanical energy at the ankle. Like other powered prostheses, the proposed underactuated mechanism uses a spring in series with the motor (Figure 1). The proposed spring assembly is uniquely integrated with the ballscrew nut to achieve a lightweight (~125 g) and compact design (30-mm outer diameter) that fits into the narrow foot shell used for our prototype (40-mm width). The proposed compliant, underactuated mechanism is key to enable a lightweight and efficient powered ankle/foot prosthesis to replicate key biomechanical functions of the biological ankle and toe joint during ambulation.

Preclinical tests with three participants with an above-knee amputation showed that the Utah Bionic Leg provided gait kinematics and kinetics similar to nonamputee individuals (Table 1, Figure 6). Of note, the toe joint worked as expected from simulation during walking, and it achieved an even larger range of motion in stair descent, which was not simulated. There were some visible differences between participants in early stance phase of walking. Participant 2 showed physiological stance knee flexion with kinematics and kinetics profiles closely matching the nonamputee references (Figure 6). In contrast, Participant 1 showed a relatively small and constant stance knee flexion angle, and Participant 3 kept the knee fully extended against the mechanical end stop throughout early stance. Abnormal stance-knee flexion is often observed in prosthetics (56–58), and is due to habitual compensatory movements used by individuals with an amputation to walk with their prescribed prosthesis rather than the controls or mechanics of the Utah Bionic Leg. Furthermore, there were visible differences in the biomechanics of the Utah Bionic Leg and that of nonamputee individuals. In stair ascent, the powered ankle prosthesis did not actively push-off, leading to visible differences in ankle kinetics (Figure 6). These differences were due to the controller in use (68) which did not implement ankle push-off, rather than the powered prosthesis mechanics. In stair descent, the powered prosthetic ankle provided lower torque than the biological ankle (Figure 6). The ankle resistive torque was set during pilot tests based on the feedback received from the participants. Thus, the observed difference was due to subjective preference rather than the prosthesis mechanics. Despite these limitations, the preliminary clinical validation showed the potential of the proposed powered prosthesis to replicate the key biomechanical functions of the biological leg during walking, stair ascent, and stair descent.

In standard mode, the Utah Bionic Leg was expected to allow for 15,460 steps on single battery charge. This number was higher than the average steps taken by individuals with lower-limb amputation (1,500 (70)) and nonamputee individuals (7,500–10,000 (69)). Thus, the experiments suggest that the Utah Bionic Leg could support multiple days of use on a

single battery charge, like microprocessor-controlled prostheses. However, it is worth noting that kinematics, kinetics, and net-energy injection change with walking speed in nonamputee individuals (73). This speed-dependent behavior could be replicated in a powered prosthesis (74) and may have a substantial effect on electrical energy consumption and battery life. When the Utah Bionic Leg was set to replicate the biomechanical functions of a passive prosthesis with a microprocessor-controlled knee (75) (Figure 6), the mechanical energy dissipation at the knee joint resulted in the Utah Bionic Leg regenerating 2.0 J of electrical energy per stride. In this passive mode, a user could walk indefinitely even if the battery was depleted. This functionality is essential to real-world viability because users may not have access to a charger or may forget to charge the prosthesis. Thus, the Utah Bionic Leg offers functionality that is not currently available to individuals with above-knee amputation.

Simulations show that increasing the range of motion of the torque-sensitive actuator would have resulted in better performance. However, in the current knee implementation, the range of motion of the torque-sensitive joint is limited to keep the overall knee dimensions comparable to a microprocessor-controlled knee, resulting in suboptimal performance (Figure 1). To reduce the negative effects of the suboptimal range of motion, we selected a relatively compliant spring, which causes the torque-sensitive joint to saturate before the maximum knee torque is achieved. Due to the saturation, the spring deflection cannot be used to measure the knee torque. Therefore, we could not implement closed-loop torque control. Bench-top tests against an external load cell show that the performance of the open-loop knee torque controller is adequate for a powered prosthesis. However, this result likely depends on the low friction and inertia of the current knee implementation and may not generalize. Also, the performance of the open-loop torque controller may degrade with time as the system friction and damping change.

The analytical model also shows that a torque-sensitive actuator can store and release energy during ambulation, theoretically reducing the required mechanical power at the motor. However, in the current implementation, we use a small, lightweight spring compared to series-elastic actuators with a similar output torque (20 g versus 200–500 g (11, 56)). As a result, energy storage and release are negligible (Figure S9). Another limitation is that the proposed torque-sensitive actuator increases the torque ratio only in response to extension knee torque (Figure 7). This unidirectional torque sensitivity does not have a negative effect on the knee performance because the biological knee flexion torque is substantially smaller than the knee extension torque during ambulation (Figure 2.A). However, there is no obvious way to achieve bidirectional torque sensitivity with the proposed design. Therefore, the benefits of the proposed torque-sensitive actuator are more substantial in joints like the biological knee or the ankle, which show a marked bias in torque. Thus, there are limitations related to the dimensions, energy efficiency, torque sensing, and sensitivity that can be achieved with the proposed torque-sensitive actuator. These limitations should be considered in future studies aiming to use the proposed torque-sensitive actuator.

The proposed underactuated toe-ankle mechanism enables the development of a lighter and more efficient ankle/foot prosthesis compared to using two separate actuators. However, it cannot provide independent control of the ankle and toe joint. Thus, a key limitation of the underactuated design is that the ratio between the ankle and toe torque is fixed

and cannot be changed based on the user's needs or preference. Moreover, even with an underactuated design, adding a toe joint increases the prosthesis weight (approximately 100 g). Comparative tests with and without the toe joint or with different ankle/toe torque ratios are necessary to assess the effect of the toe joint on clinical outcomes. These clinical studies are necessary to justify the use of an articulated toe joint. Moreover, simulations show that a more compliant spring would have improved dynamic performance and electrical efficiency. However, it would have required a longer spring, which would have reduced the range of motion of the ankle and toe joints. These limitations are inherent to the proposed underactuated toe-ankle mechanism and should be considered in future designs.

Similar to most microprocessor-controlled and powered ankle/foot prostheses, the proposed ankle design does not have actuation in the frontal plane. Adding the frontal plane actuation is likely to increase the size and weight of the prosthesis. However, it may also improve clinical outcomes, especially when walking on inclines and rough terrains. Powered emulators (76, 77) and prostheses (78, 79) with passive or active frontal plane actuation have been developed to study the effectiveness of frontal plane actuation. Future work should consider implementing frontal plane actuation based on the outcome of these studies.

This design-validation study shows that the Utah Bionic Leg has the potential to replicate the key biomechanical functions of the missing biological leg for participants spanning large ranges of height (160–191 cm) and body weight (59–91 kg without the prosthesis). Our results suggest that the performance of the Utah Bionic Leg is appropriate for clinical studies assessing biomechanics and clinical outcomes in a statistically significant number of participants. Leveraging the modularity of our powered prosthesis, these clinical studies should assess the contribution of the three powered joints—the knee, the ankle, and the toe—to amputee mobility and subjective preference.

By replicating key biomechanical functions of the missing biological leg, robotic leg prostheses have the potential to improve ambulation for millions of people living with an above-knee amputation (9, 80). However, excessive weight, size, and short battery life have prevented existing robotic leg prostheses to achieve clinical success. In this paper, we show that a torque-sensitive actuator can enable a small, lightweight motor to efficiently provide the wide ranges of torques and speeds required for a knee prosthesis. We also show that a compliant, underactuated system can concurrently power the toe and ankle joint, and also enable substantial mechanical energy regeneration. Combined, these design solutions enable a robotic leg prosthesis to replicate the key biomechanical functions of the biological knee, ankle, and toe in the sagittal plane and match the weight, size, and battery life of microprocessor-controlled prostheses.

By enabling the development of prostheses that are both lightweight and powered, this study provides a scientific tool to study amputee gait mechanics and improve the mobility of individuals with above-knee amputations in real life. The Utah Bionic Leg can enable scientists to study both the effects of energy injection and the effect of active control on amputee gait mechanics without the confounding effect of prosthesis weight. Moreover, leveraging its lightweight design, future studies using the Utah Bionic Leg could include elderly and dysvascular participants, who lack the strength and balance required to use

heavier powered devices. Moreover, the Utah Bionic Leg satisfies basic requirements for use at home. Thus, it may enable researchers to conduct studies outside the laboratory space, expanding the landscape of powered prosthesis research.

Materials and Methods

Knee Design

The proposed torque-sensitive actuator comprises two closed kinematic chains connected in parallel. The first kinematic chain has five joints in closed configuration $(P_1R_2R_3P_2R_1P_1R_2R_3P_2R_1)$ creating a five-bar mechanism with two degrees of freedom, where R_1 is the output knee joint, P_1 is the input joint powered by a linear actuator, and P_2 is the torque-sensitive joint (Figure 7.A). The torque-sensitive joint (P_2) connects to a prismatic joint (P_3) in the second kinematic chain ($R_4P_3R_3P_2R_1$), which is passively actuated by a tension spring (Figure 7.B). The position of the torque-sensitive joint (P_2) affects the relationship between the force at the input joint (P_1) and torque at the output joint (R_1), effectively regulating the torque ratio of the actuator (the ratio between output torque and input force). More importantly, due to the connection with the spring-loaded joint (P_3), the position of the torque-sensitive joint (P_2) depends on the force on the input joint (P_1). As shown in Figure 7.B, when the linear actuator powering the input joint (P_1) pulls to generate extension torque at the output joint (R_1), the tension spring (P_3) extends causing the torque-sensitive joint (P_2) to move away from the output joint (R_1), increasing the moment arm of the pulling force generated by the linear actuator. Thus, the torque ratio increases passively as a function of the extension torque on the output knee joint (Figure 7.C). Due to the non-linear kinematics of the mechanism, the torque ratio also depends on the knee angle (Figure 7.C). Moreover, due to the presence of a second degree of freedom (the torque-sensitive joint), the actuator's torque ratio is not the inverse of the velocity ratio. Thus, the proposed actuator conceptually differs from continuous variable transmissions, as shown by the analytical model described in Supplementary Methods.

The proposed torque-sensitive actuator is implemented in a compact, lightweight powered knee prosthesis (Figure 7.D). The torque-sensitive actuator is fully integrated in a 7075-T6 aluminum frame, which provides structural support, protection for the mechanics and electronics, and also works as a heat sink. The prosthesis actuator comprises a DC motor, a helical gear pair, and a ball screw and nut assembly supported by two miniaturized linear guides. Passive degrees of freedom between the actuation and the frame allow for self-alignment of the actuation system. The linear actuator is connected to the torque-sensitive joint through two parallel bars, which are joined by a steel shaft. The steel shaft slides into two parallel slots in the top knee structure and connects to the spring-actuated joint, which is implemented using a tension coil spring. Video S2 shows an animation of the torque-sensitive actuation. The top knee structure connects to the user's socket with a titanium male pyramid adapter like in commercially available prostheses. Mechanical end-stops limit the range of motion of the knee joint to 0°–120° (Figure 7.F–G). The top knee structure contains an embedded electronic system that handles data processing of the absolute encoders in the knee and torque-sensitive joint as well as of the inertial measurement unit, and also provides an additional digital/analog interface for additional sensing and control modes such

as electromyography (Figure 7.E). The motherboard, located in the main knee structure, uses a microcontroller (PIC32) to run control algorithms and to communicate with the power electronic board where the motor current driver and motor chokes are located. The motherboard can host an optional embedded computer (Raspberry Pi 3+ compute module) to save data and communicate via Wi-Fi to an external laptop for data telemetry. An embedded 6-cell 1200 mAh lithium-ion battery powers the knee. The powered knee is designed based on ISO 10328 standard. More details on the mechatronic implementation are provided in the Supplementary Methods.

Ankle Design

The kinematics of the proposed underactuated system comprises five joints in closed configuration ($R_1R_2P_1R_3R_4P_1R_2R_3P_2R_1$) creating a five-bar mechanism with two degrees of freedom. As shown in Figure 8.A–B, the prismatic joint P_1 is actuated by a linear series-elastic actuator concurrently generating torque at the ankle (R_1) and the toe joint (R_4). Because the mechanical advantage of the linear actuator with respect to the ankle joint is greater than that of the toe joint ($\overline{R_1R_2} > \overline{R_3R_4}$), the ankle torque ratio is considerably bigger than the toe torque ratio (Figure 8.C). In other terms, the ankle torque is greater than the toe torque for any given force generated by the linear series-elastic actuator. Due to the non-linear kinematics of the proposed mechanism, the torque ratios depend on the joint angles, although this dependency is marginal for the proposed actuator configuration (see Supplementary Methods). Notably, a mechanical end stop limits the range of motion of the toe joint so that it cannot pass the neutral angle. In this configuration, the kinematic chain loses one degree of freedom, and the proposed actuation system is not underactuated, so the ankle joint can be controlled without affecting the toe joint. Moreover, a viscoelastic element returns the toe joint to a neutral position when no force is applied at the input joint, such as at the end of swing phase.

The proposed compliant underactuated mechanism is implemented in a lightweight, compact ankle/foot prosthesis (Figure 8.D). A linear series-elastic actuator transmits power to both the toe joint and the ankle joint, through the pivot joints implemented in the toe and shank frame. The linear series-elastic actuator comprises an electrical motor, a ballscrew with integrated nut-spring assembly, and a custom gearbox, with bevel and helical gears. The ballscrew is located inside the carbon-fiber foot shell taken from a commercially available ankle/foot prosthesis (Ottobock Meridium), whereas an electrical motor is located inside the shank frame, which is machined out of 7075-T6 aluminum and provides structural support, protection, and heat sink capacity. The custom gearbox enables the electrical motor to remain in a fixed position with respect to the shank frame while the ankle and toe joint move, using a set of three bevel gears. The first gear is coaxial to the ball screw axis of rotation and transmits power to the ball screw and the second gear. The second gear spins freely and is coaxial with the pivot joint R3 on the shank frame (Figure 8.B). The third gear transfers power between the second gear and the motor shaft. The range of motion of the ankle and toe joint is 40° (+/−20°) and 45°, respectively (Figure 8.F–G). Absolute magnetic encoders measure the angles of the ankle and the toe joint. A linear potentiometer measures the length of the spring. A custom instrumented pyramid provides ground reaction force sensing(55). A 9-axis inertial measurement unit is integrated into the foot shell to determine

the foot orientation in space. The sensor outputs are processed by a dedicated embedded electronic system while another embedded electronic system runs all the control routines and communicates with the power electronic board, which hosts the motor driver. An embedded 6-cell 1200 mAh lithium-ion battery powers the ankle/foot. The knee and ankle modules communicate using a serial peripheral interface, which runs inside the pylon so there are no electrical wires exposed (Figure S7). The proposed ankle/foot is designed based on ISO 10328 standard (see Supplementary Methods). Our powered ankle/foot prosthesis leverages the proposed compliant underactuated mechanism to satisfy similar weight and size requirements to microprocessor-controlled ankle/foot prostheses, and actively powers both the ankle and toe joints during ambulation.

Modeling and Dynamic Simulations

We used a simulation framework to support the design of the torque-sensitive actuator and the compliant underactuated system. The framework was used to solve the system dynamics and calculate the motor torque, speed, voltage, and current necessary to generate physiological torque and velocity at the knee or ankle joint during ambulation (Figure 2.A). Additionally, the framework was used to calculate the position, velocity, force and torque on each mechanical element of the design. The framework used a brute-force optimization approach, which explores the whole design space within defined ranges of the kinematic and actuator parameters (Tables S2 and S3). The solutions were tested against several hard limits to assess feasibility. The battery voltage defined a hard limit for the instantaneous motor torque/speed combination. Moreover, the ability of the motor to dissipate heat defined a hard limit for the continuous current and torque that an electrical motor can safely provide without overheating. We also included hard limits on force/torque/speed of other joints, which require bearings, linear guides, or ball screws. We simulated several brushless motors that could fit within the desired prosthesis dimension. Moreover, for each motor, we simulated several winding configurations in combination with different battery voltages, below and above the nominal voltage specified in the motor datasheet. Finally, we selected the motor/winding/battery combination with the smallest total mass based on the estimates provided by the simulation framework. The framework is presented in detail in the Supplementary Methods. The simulation framework was essential to engineer the torque-sensitive actuator and the compliant underactuated system because the torque ratio depends non-linearly on both the output joint position and torque. Therefore, it might not have been possible to find the proposed design solutions based solely on the intuition of the designer.

Bench-top testing

The knee and ankle/foot module were tested separately on the bench. Each module underwent multiple experiments using either a fully constrained or partially constrained setup. For the fully constrained setup, both the proximal and distal links of the module were mechanically grounded to a testing jig, which served to prevent movement and provide reaction forces and moments. For the partially constrained setup, one link of the module was mechanically grounded to a testing jig, and the remaining link was free to rotate. During experiments that require readings of output joint torque, a six-axis load cell (Sunrise Instruments, M3713D) was connected in series with the proximal portion of the module.

To quantify the position response of the knee and ankle modules, we performed closed-loop position step response experiments with a partially constrained setup. We tested with three levels of reference step position (5, 10, and 15°) for both modules, and each level was tested five times. We recorded joint angle over time. To quantify the torque response of the knee and ankle/foot modules, we performed open-loop torque step response experiments with a fully constrained setup. We tested with four levels of reference step torque ($\pm$ 20 Nm, $\pm$ 40 Nm) for both modules, and each level was tested five times. We recorded joint torque and motor current over time. To quantify the passive behavior of the knee and ankle/foot modules, we performed manual backdriving experiments with a partially constrained setup. For each module, with the motor turned off, an experimenter manually moved the output joint through its range of motion in two sessions. In the first session, we slowly backdrove each module (~ 0.1 Hz), to quantify the minimum backdriving torque. In the second session, we backdrove each module with frequencies continuously varying from 0.2 Hz-1.5 Hz. The joint torque and position data of this experiment were then used as inputs to the System Identification toolbox in Matlab, which estimated the joint's reflected damping and inertia parameters using a two-pole one-zero model.

To demonstrate the behavior of the knee module's torque sensitive transmission in high-torque dynamic tasks, we generated bell-shaped joint torque profiles used in the stance phase of reciprocal stair climbing, with a partially constrained setup. The peak torque was scaled to 90 Nm, and we performed testing with the torque sensitive joint unlocked and locked at its minimum position. For each condition, we repeated the test five times. We recorded joint torque, joint angle and motor current. In addition, to demonstrate the behavior of the knee module's torque sensitive transmission in high-speed dynamic tasks, we commanded two minimum-jerk position profiles that represented those during walking and stair ascent ambulation, with a partially constrained setup. We performed testing with the torque sensitive joint unlocked and locked at its maximum position. For each condition, we repeat the test five times. We record desired and measured joint position over time.

To demonstrate the effect of the underactuated ankle-toe mechanism on the linear actuator, we commanded the ankle joint to generate a 0.5 Hz sinusoidal position profile with a partially constrained setup. We performed testing under two conditions: with the toe joint locked, and with the toe joint manually synchronized with the ankle motion to minimize linear actuator movement by the experimenter. For each condition, we tested three times. We recorded joint positions, and the movement of the linear actuator.

To quantify the stiffness of the series spring of the ankle/foot module, we constructed a custom jig to load the spring subassembly in both tension and compression. One end of the spring subassembly was mechanically grounded to the jig and connected in series to the 6-axis load cell, and the other end was manually loaded by the experimenter through a four-bar linkage leverage. For each loading direction, we performed three cycles of loading-unloading from 0 to 400 N. We recorded the force and linear displacement of the spring and used linear regression to estimate the spring stiffness.

To quantify the thermal response of the knee and ankle/foot modules, we supplied a constant current through the motor with a fully constrained setup. We measured the device

temperature with a thermocouple (Mouser 410–315) placed on the prosthesis frame, close to the motor housing. The thermocouple readings were confirmed using a thermal camera (FLIR ONE). We supplied two levels of current to the motor: the nominal current as specified in the motor datasheet for 60 minutes, and a higher level of current for 10 minutes. The actual current was verified using direct measurements from the motor driver. We recorded prosthesis temperature and used thermal modelling (see Supplementary Methods) to determine the improved continuous and short-term current limits of the motor-frame assembly for each module.

Amputee Testing Protocol

We recruited three individuals with above-knee amputation (34±6 years old, 72±16 kg body mass, Figure 5) for this study, and all participants provided written consent to University of Utah's IRB-approved clinical testing protocols. For data collection, the participants were fitted to the powered leg by a certified prosthetist, and then ambulated on level-ground and stairs, all in one test session. Level-ground walking was performed on the treadmill at a speed of 1.25 m/s, and stair ascent (both step-over-step and 2 steps at a time) and descent were performed with a reciprocal pattern. The participants had different levels of experience with the Utah Bionic Leg prior to data collection. Participant 1 had about 20 hours of experience with the Utah Bionic Leg as he was involved in the early development of the device and related ambulation controllers. Participant 2 had two hours of experience, gained during a familiarization session performed the week before data collection. Participant 3 did not have any experience before the data collection session. So, he was given a few minutes to practice before we started recording data and videos. Additional participant information is available in Table S5. We processed the testing data offline as explained in detail in the Supplementary Methods.

To accurately assess electrical energy consumption, we performed an additional test with Participant 1. For this test, we configured the Utah Bionic Leg to use a single Li-Ion battery (6-cell, 1600 mAh). After calibration, current and voltage sensors were added directly at the battery leads. We enclosed the battery and sensors in a dedicated 3D-printed plastic cover connected to the back of the knee module. We acquired the sensor outputs in real-time using the embedded knee electronics (Figure S11). The participant walked on the treadmill at 1.25 m/s in both standard mode and passive mode, while we recorded the battery voltage and current. We calculated the electrical battery power offline by multiplying the measured battery voltage and current. Also, we calculated the electrical energy offline by integrating the electrical power over time for each stride. Then, we normalized the electrical energy consumption by the participant's body weight and calculated the average during standard and passive mode separately.

Control Architecture

For all amputee experiments, we used ambulation controllers that were previously validated with above-knee amputee participants (walking (74, 81), stair ascent (68), stair descent (45)). During the experiments, we switched between the ambulation controllers manually, using a graphical user interface. Although the ambulation controllers were designed to provide the powered prosthesis with different functionalities, they shared a common

hierarchical control architecture (Figure S15). At the higher level, there was a finite-state machine with two states: *Stance* and *Swing*. The transition rules between these two states were specific to each ambulation controller and can be found in previous publications (45, 68, 74, 81). *Stance* and *Swing* used different control algorithms, implemented in the mid-level controller. In *Swing*, we used a position controller. The position controller defined a desired position either using a minimum-jerk optimization (74) or based on the movements of the user's residual limb (68). This approach allowed for smooth transitions between *Stance* and *Swing* in all conditions as well as for indirect volitional control of the prosthesis behavior (81). In *Stance*, we used a torque controller. The torque controller defined a desired joint torque based on quasi-stiffness profiles (82)extracted from able-bodied datasets of ambulation biomechanics and implemented using look-up tables for maximal computational efficiency (74). This approach enabled the prosthesis to provide biologically accurate torque as the user walked at variable speeds and cadences (74) or climb stairs with different stair heights or gait pattens (68) and required minimal (68) to no participant-specific tuning (74). The desired torque or position were fed to dedicated low-level controllers, which generate current commands for the knee and ankle motor drivers. For both the knee and ankle/foot modules, the position controller was based on a simple proportional-derivative (PD) compensator with additional feed-forward terms for gravity and friction compensation (45). The knee module used an open loop torque controller (Figure S14), which defined the desired current based on an online estimate of the torque ratio using the torque-sensitive model shown in the Supplementary Methods, as well as dynamic damping and inertia compensators similar to our previous powered prostheses (18, 45). In contrast, the ankle/foot module used a closed-loop torque controller (Figure S14) with a PD compensator closing the loop on the online measurement of torque based on the series-spring deflection, as well as an online estimate of the ankle torque ratio based on the ankle and toe encoder readings.

Statistics

For important quantitative metrics related to benchtop and amputee participant testing, we calculated mean values (± standard deviation). Within amputee testing data, each subsample represents one stride (segmented from heel-strike to heel-strike) from a given participant and ambulation mode. To obtain fitted curves to characterize the ankle/foot spring and thermal properties of the device, we used the Curve Fitting Toolbox in Matlab and obtained R^2 values of at least 0.95.

Supplementary Material

Refer to Web version on PubMed Central for supplementary material.

Acknowledgments

Data and materials availability:

All data needed to evaluate the conclusions of the paper are available in the paper or the Supplementary Materials.

REFERENCES

1. Versluys R, Beyl P, van Damme M, Desomer A, van Ham R, Lefeber D, Prosthetic feet: State-of-the-art review and the importance of mimicking human anklefoot biomechanics. Disabil Rehabil Assist Technol. 4 (2009),, doi:10.1080/17483100802715092.

2. Hahn A, Sreckovic I, Reiter S, Mileusnic M, First results concerning the safety, walking, and satisfaction with an innovative, microprocessor-controlled four-axes prosthetic foot. Prosthet Orthot Int. 42 (2018), doi:10.1177/0309364617747976.

3. Michael JW, "Modern prosthetic knee mechanisms" in Clinical Orthopaedics and Related Research (1999), vol. 361.

4. Thiele J, Schöllig C, Bellmann M, Kraft M, Designs and performance of three new microprocessor-controlled knee joints. Biomedical Engineering / Biomedizinische Technik (2018), doi:10.1515/bmt-2017-0053.

5. Goldfarb M, Consideration of Powered Prosthetic Components as They Relate to Microprocessor Knee Systems. JPO Journal of Prosthetics and Orthotics. 25, P65–P75 (2013).

6. Winter DA, Energy generation and absorption at the ankle and knee during fast, natural, and slow cadences. Clin Orthop Relat Res (1983), doi:10.1097/00003086-198305000-00021.

7. McFadyen BJ, Winter DA, An integrated biomechanical analysis of normal stair ascent and descent. J Biomech (1988), doi:10.1016/0021-9290(88)90282-5.

8. Schmalz T, Blumentritt S, Jarasch R, Energy expenditure and biomechanical characteristics of lower limb amputee gait: Gait Posture. 16 (2002), doi:10.1016/s0966-6362(02)00008-5.

9. Wurdeman SR, Stevens PM, Campbell JH, Mobility Analysis of AmpuTees (MAAT I): Quality of life and satisfaction are strongly related to mobility for patients with a lower limb prosthesis. Prosthet Orthot Int. 42 (2018), doi:10.1177/0309364617736089.

10. Goldfarb M, Lawson BE, Shultz AH, Realizing the promise of robotic leg prostheses. Sci Transl Med (2013),, doi:10.1126/scitranslmed.3007312.

11. Rouse EJ, Mooney LM, Herr HM, Clutchable series-elastic actuator: Implications for prosthetic knee design. International Journal of Robotics Research (2014), doi:10.1177/0278364914545673.

12. Pfeifer S, Pagel A, Riener R, Vallery H, Actuator With Angle-Dependent Elasticity for Biomimetic Transfemoral Prostheses. Mechatronics, IEEE/ASME Transactions on. PP, 1–11 (2014).

13. Flynn L, Geeroms J, Jimenez-Fabian R, Vanderborght B, Vitiello N, Lefeber D, Ankle-knee prosthesis with active ankle and energy transfer: Development of the CYBERLEGs Alpha-Prosthesis. Rob Auton Syst. 73, 4–15 (2015).

14. Martinez-Villalpando E, Herr H, Agonist-antagonist active knee prosthesis: A preliminary study in level-ground walking. J Rehabil Res Dev. 46, 361–373 (2009). [PubMed: 19675988]

15. Elery T, Rezazadeh S, Nesler C, Doan J, Zhu H, Gregg RD, Design and Benchtop Validation of a Powered Knee-Ankle Prosthesis with High-Torque, Low-Impedance Actuators. IEEE Int. Conf. Robot. Automat, 2788–2795 (2018).

16. Bellman AHR and Sugar T, Bellman RD, Holgate MA, Sugar TG, SPARKy 3: Design of an active robotic ankle prosthesis with two actuated degrees of freedom using regenerative kinetics. Proc. IEEE/RAS-EMBS Int. Conf. on Biomedical Robotics and Biomechatronics, 511–516 (2008).

17. Au SK, Herr HM, Powered ankle-foot prosthesis. IEEE Robot Autom Mag. 15, 52–59 (2008).

18. Gabert L, Hood S, Tran M, Cempini M, Lenzi T, A compact, lightweight robotic ankle-foot prosthesis: Featuring a powered polycentric design. IEEE Robot Autom Mag. 27 (2020), doi:10.1109/MRA.2019.2955740.

19. Au SK, Weber J, Herr H, Powered Ankle--Foot Prosthesis Improves Walking Metabolic Economy. IEEE Transactions on Robotics. 25, 51–66 (2009).

20. Feng Y, Mai J, Agrawal SK, Wang Q, Energy regeneration from electromagnetic induction by human dynamics for lower extremity robotic prostheses. IEEE Transactions on Robotics. 36 (2020), doi:10.1109/TRO.2020.2991969.

21. Cherelle P, Grosu V, Matthys A, Vanderborght B, Lefeber D, Design and validation of the ankle mimicking prosthetic (AMP-) Foot 2.0. IEEE Transactions on Neural Systems and Rehabilitation Engineering. 22 (2014), doi:10.1109/TNSRE.2013.2282416.

22. Cherelle P, Grosu V, Flynn L, Junius K, Moltedo M, Vanderborght B, Lefeber D, The Ankle Mimicking Prosthetic Foot 3—Locking mechanisms, actuator design, control and experiments with an amputee. Rob Auton Syst. 91 (2017), doi:10.1016/j.robot.2017.02.004.

23. Ottobock Empower (2019), (available at https://www.ottobockus.com/prosthetics/lower-limb-prosthetics/solution-overview/empower-ankle/).

24. Ossur, OSSUR, The POWER KNEE, (available at http://bionics.ossur.com/Products/POWER-KNEE/SENSE).

25. Kim J, Wensman J, Colabianchi N, Gates DH, The influence of powered prostheses on user perspectives, metabolics, and activity: a randomized crossover trial. J Neuroeng Rehabil. 18 (2021), doi:10.1186/s12984-021-00842-2.

26. Gardinier ES, Kelly BM, Wensman J, Gates DH, A controlled clinical trial of a clinically-tuned powered ankle prosthesis in people with transtibial amputation. Clin Rehabil. 32 (2018), doi:10.1177/0269215517723054.

27. Lechler K, Frossard B, Whelan L, Langlois D, Müller R, Kristjansson K, Motorized Biomechatronic Upper and Lower Limb Prostheses—Clinically Relevant Outcomes. PM and R. 10 (2018),, doi:10.1016/j.pmrj.2018.06.015.

28. Hafner BJ, Askew RL, Physical performance and self-report outcomes associated with use of passive, adaptive, and active prosthetic knees in persons with unilateral, transfemoral amputation: Randomized crossover trial. J Rehabil Res Dev. 52, 677–700 (2015). [PubMed: 26560243]

29. Smith JD, Martin PE, Effects of Prosthetic Mass Distribution on Metabolic Costs and Walking Symmetry. J Appl Biomech (2012).

30. Smith JD, Martin PE, Short and Longer Term Changes in Amputee Walking Patterns Due to Increased Prosthesis Inertia. JPO Journal of Prosthetics and Orthotics. 23, 114–123 (2011).

31. Narang YS, Arelekatti VNM, Winter AG, The Effects of Prosthesis Inertial Properties on Prosthetic Knee Moment and Hip Energetics Required to Achieve Able-Bodied Kinematics. IEEE Transactions on Neural Systems and Rehabilitation Engineering. 24 (2016), doi:10.1109/TNSRE.2015.2455054.

32. Baimyshev A, Lawson B, Goldfarb M, "Design and Preliminary Assessment of Lightweight Swing-Assist Knee Prosthesis" in 2018 40th Annual International Conference of the IEEE Engineering in Medicine and Biology Society (EMBC) (IEEE, 2018), pp. 3198–3201.

33. Lenzi T, Sensinger J, Lipsey J, Hargrove L, Kuiken T, "Design and preliminary testing of the RIC hybrid knee prosthesis" in Proceedings of the Annual International Conference of the IEEE Engineering in Medicine and Biology Society, EMBS (2015).

34. Lenzi T, Cempini M, Hargrove L, Kuiken T, "Hybrid actuation systems for lightweight transfemoral prostheses" in Frontiers in Biomedical Devices, BIOMED - 2017 Design of Medical Devices Conference, DMD 2017 (2017).

35. Lenzi T, Cempini M, Hargrove L, Kuiken T, Design, development, and testing of a lightweight hybrid robotic knee prosthesis. International Journal of Robotics Research (2018), doi:10.1177/0278364918785993.

36. Shepherd MK, Rouse EJ, The VSPA Foot: A Quasi-Passive Ankle-Foot Prosthesis with Continuously Variable Stiffness. 4320 (2017), doi:10.1109/TNSRE.2017.2750113.

37. Lecomte C, Ármannsdóttir AL, Starker F, Tryggvason H, Briem K, Brynjolfsson S, Variable stiffness foot design and validation. J Biomech. 122 (2021), doi:10.1016/j.jbiomech.2021.110440.

38. Lenzi T, Cempini M, Newkirk J, Hargrove LJ, Kuiken TA, "A lightweight robotic ankle prosthesis with non-backdrivable cam-based transmission" in IEEE International Conference on Rehabilitation Robotics (2017).

39. Glanzer EM, Adamczyk PG, Design and Validation of a Semi-Active Variable Stiffness Foot Prosthesis. IEEE Transactions on Neural Systems and Rehabilitation Engineering. 26 (2018), doi:10.1109/TNSRE.2018.2877962.

40. Bartlett HL, King ST, Goldfarb M, Lawson BE, A Semi-Powered Ankle Prosthesis and Unified Controller for Level and Sloped Walking. IEEE Transactions on Neural Systems and Rehabilitation Engineering. 29 (2021), doi:10.1109/TNSRE.2021.3049194.

41. Gao S, Mai J, Zhu J, Wang Q, Mechanism and Controller Design of a Transfemoral Prosthesis with Electrohydraulic Knee and Motor-Driven Ankle. IEEE/ASME Transactions on Mechatronics. 26 (2021), doi:10.1109/TMECH.2020.3040369.

42. Lenzi T, Cempini M, Hargrove LJ, Kuiken TA, Design, Development, and Validation of a Lightweight Nonbackdrivable Robotic Ankle Prosthesis. IEEE/ASME Transactions on Mechatronics. 24 (2019), doi:10.1109/TMECH.2019.2892609.

43. VARIABLE TRANSMISSION FOR ASSISTIVE PROSTHESIS DEVICE (2020), (available at https://patentscope.wipo.int/search/en/detail.jsf?docId=WO2020047043).

44. Lenzi T, Cempini M, Hargrove LJ, Kuiken TA, Actively variable transmission for robotic knee prostheses. 2017 IEEE International Conference on Robotics and Automation (ICRA), 6665–6671 (2017).

45. Tran M, Gabert L, Cempini M, Lenzi T, A Lightweight, Efficient Fully Powered Knee Prosthesis with Actively Variable Transmission. IEEE Robot Autom Lett. 4, 1186–1193 (2019).

46. Mager F, Richards J, Hennies M, Dötzel E, Chohan A, Mbuli A, Capanni F, Determination of ankle and metatarsophalangeal stiffness during walking and jogging. J Appl Biomech. 34 (2018), doi:10.1123/jab.2017-0265.

47. DeFrino PF, Brodsky JW, Polio FE, Crenshaw SJ, Beischer AD, First metatarsophalangeal arthrodesis: A clinical, pedobarographic and gait analysis study. Foot Ankle Int. 23 (2002), doi:10.1177/107110070202300605.

48. Honert EC, Bastas G, Zelik KE, Effect of toe joint stiffness and toe shape on walking biomechanics. Bioinspir Biomim. 13 (2018), doi:10.1088/1748-3190/aadf46.

49. Grabowski AM, Rifkin J, Kram R, K3 promoter™ prosthetic foot reduces the metabolic cost of walking for unilateral transtibial amputees. Journal of Prosthetics and Orthotics. 22 (2010), doi:10.1097/JPO.0b013e3181cca79c.

50. Zhu J, Wang Q, Wang L, On the design of a powered transtibial prosthesis with stiffness adaptable ankle and toe joints. IEEE Transactions on Industrial Electronics. 61 (2014), doi:10.1109/TIE.2013.2293691.

51. Zhu J, She H, Huang Q, "Pantoe II: Improved version of a powered transtibial prosthesis with ankle and toe joints" in Frontiers in Biomedical Devices, BIOMED - 2018 Design of Medical Devices Conference, DMD 2018 (2018).

52. Laffranchi M, Boccardo N, Traverso S, Lombardi L, Canepa M, Lince A, Semprini M, Saglia JA, Naceri A, Sacchetti R, Gruppioni E, de Michieli L, The Hannes hand prosthesis replicates the key biological properties of the human hand. Sci Robot. 5 (2020), doi:10.1126/SCIROBOTICS.ABB0467.

53. Ottobock Genium X3, (available at https://professionals.ottobockus.com/Prosthetics/Lower-Limb-Prosthetics/Knees--Microprocessor/X3/Genium-X3/p/3B5-2~5ST).

54. Otto Bock Meridium Product Page, (available at https://shop.ottobock.us/Prosthetics/Lower-Limb-Prosthetics/Feet---Microprocessor/Meridium/p/1B1).

55. Gabert L, Lenzi T, Instrumented Pyramid Adapter for Amputee Gait Analysis and Powered Prosthesis Control. IEEE Sens J. 19 (2019), doi:10.1109/JSEN.2019.2920179.

56. Azocar AF, Mooney LM, Duval JF, Simon AM, Hargrove LJ, Rouse EJ, Design and clinical implementation of an open-source bionic leg. Nat Biomed Eng. 4 (2020), doi:10.1038/s41551-020-00619-3.

57. Lawson BE, Mitchell J, Truex D, Shultz A, Ledoux E, Goldfarb M, A robotic leg prosthesis: Design, control, and implementation. IEEE Robot Autom Mag. 21, 70–81 (2014).

58. Elery T, Rezazadeh S, Nesler C, Gregg RD, Design and validation of a powered knee-ankle prosthesis with high-torque, low-impedance actuators. IEEE Transactions on Robotics. 36, 1649–1668 (2020). [PubMed: 33299386]

59. Hunter I, Hollerbach JM, Ballantyne J, A comparative analysis of actuator technologies for robotics. Robotics Review 2 (1991).

60. O'Brien KW, Xu PA, Levine DJ, Aubin CA, Yang HJ, Xiao MF, Wiesner LW, Shepherd RF, Elastomeric passive transmission for autonomous force-velocity adaptation applied to 3D-printed prosthetics. Sci Robot (2018), doi:10.1126/scirobotics.aau5543.

61. Crenna F, Rossi GB, Berardengo M, Filtering biomechanical signals in movement analysis. Sensors. 21 (2021), doi:10.3390/s21134580.

62. Zhu J, Jiao C, Dominguez I, Yu S, Su H, Design and Backdrivability Modeling of a Portable High Torque Robotic Knee Prosthesis With Intrinsic Compliance for Agile Activities. IEEE/ASME Transactions on Mechatronics. 27, 1837–1845 (2022).

63. Weight Percentile Calculator for Men and Women in the United States, (available at https://dqydj.com/weight-percentile-calculator-men-women/).

64. Winter DA, Biomechanics and Motor Control of Human Movement: Fourth Edition (2009).

65. Bruening DA, Cooney KM, Buczek FL, Analysis of a kinetic multi-segment foot model. Part I: Model repeatability and kinematic validity. Gait Posture. 35 (2012), doi:10.1016/j.gaitpost.2011.10.363.

66. Bruening DA, Cooney KM, Buczek FL, Analysis of a kinetic multi-segment foot model part II: Kinetics and clinical implications. Gait Posture. 35 (2012), doi:10.1016/j.gaitpost.2011.11.012.

67. Riener R, Rabuffetti M, Frigo C, Stair ascent and descent at different inclinations. Gait Posture (2002), doi:10.1016/S0966-6362(01)00162-X.

68. Hood S, Gabert L, Lenzi T, Powered Knee and Ankle Prosthesis With Adaptive Control Enables Climbing Stairs With Different Stair Heights, Cadences, and Gait Patterns. IEEE Transactions on Robotics. 38 (2022), doi:10.1109/TRO.2022.3152134.

69. Tudor-Locke C, Craig CL, Brown WJ, Clemes SA, de Cocker K, Giles-Corti B, Hatano Y, Inoue S, Matsudo SM, Mutrie N, Oppert JM, Rowe DA, Schmidt MD, Schofield GM, Spence JC, Teixeira PJ, Tully MA, Blair SN, How many steps/day are enough? for adults. International Journal of Behavioral Nutrition and Physical Activity. 8 (2011), doi:10.1186/1479-5868-8-79.

70. Halsne EG, Waddingham MG, Hafner BJ, Long-term activity in and among persons with transfemoral amputation. J Rehabil Res Dev 50 (2013), doi:10.1682/JRRD.2012.04.0066.

71. Pratt GA, Williamson MM, "Series elastic actuators" in IEEE International Conference on Intelligent Robots and Systems (1995).

72. Browning RC, Modica JR, Kram R, Goswami A, The effects of adding mass to the legs on the energetics and biomechanics of walking. Med Sci Sports Exerc (2007), doi:10.1249/mss.0b013e31802b3562.

73. Hansen AH, Childress DS, Miff SC, Gard SA, Mesplay KP, The human ankle during walking: Implications for design of biomimetic ankle prostheses. J Biomech. 37 (2004), doi:10.1016/j.jbiomech.2004.01.017.

74. Lenzi T, Hargrove L, Sensinger J, Speed-adaptation mechanism: Robotic prostheses can actively regulate joint torque. IEEE Robot Autom Mag. 21, 94–107 (2014).

75. Hood S, Ishmael MK, Gunnell A, Foreman KB, Lenzi T, A kinematic and kinetic dataset of 18 above-knee amputees walking at various speeds. Sci Data. 7 (2020), doi:10.1038/s41597-020-0494-7.

76. Kim M, Lyness H, Chen T, Collins SH, The Effects of Prosthesis Inversion/Eversion Stiffness on Balance-Related Variability during Level Walking: A Pilot Study. J Biomech Eng. 142 (2020), doi:10.1115/1.4046881.

77. Kim M, Collins SH, Step-to-step ankle inversion/eversion torque modulation can reduce effort associated with balance. Front Neurorobot. 11 (2017), doi:10.3389/fnbot.2017.00062.

78. Rogers EA, Carney ME, Yeon SH, Clites TR, Solav D, Herr HM, An Ankle-Foot Prosthesis for Rock Climbing Augmentation. IEEE Transactions on Neural Systems and Rehabilitation Engineering. 29 (2021), doi:10.1109/TNSRE.2020.3033474.

79. Ficanha EM, Ribeiro GA, Dallali H, Rastgaar M, Design and preliminary evaluation of a two DOFs cable-driven ankle-foot prosthesis with active dorsiflexion-plantarflexion and inversion-eversion. Front Bioeng Biotechnol. 4 (2016), doi:10.3389/fbioe.2016.00036.

80. Sinha R, van den Heuvel WJA, Arokiasamy P, Factors affecting quality of life in lower limb amputees. Prosthet Orthot Int. 35 (2011), doi:10.1177/0309364610397087.

81. Mendez J, Hood S, Gunnel A, Lenzi T, Powered knee and ankle prosthesis with indirect volitional swing control enables level-ground walking and crossing over obstacles. Sci Robot. 5 (2020), doi:10.1126/scirobotics.aba6635.

82. Rouse EJ, Gregg RD, Hargrove LJ, Sensinger JW, The difference between stiffness and quasi-stiffness in the context of biomechanical modeling. IEEE Trans Biomed Eng. 60 (2013), doi:10.1109/TBME.2012.2230261.
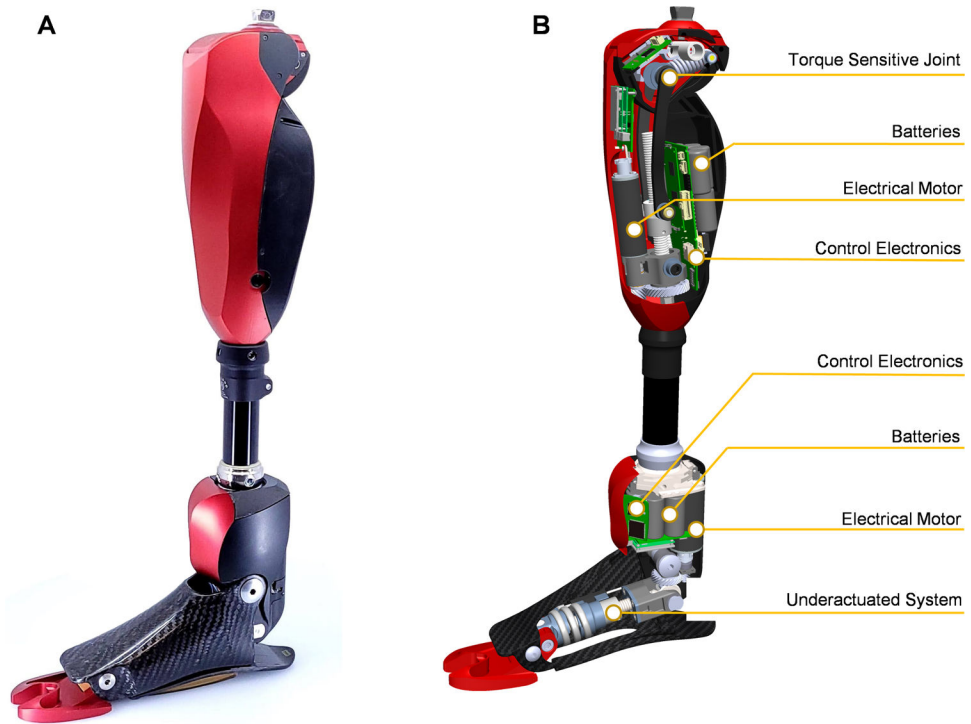
Figure 1. System Overview

(**A**) A photo of the Utah Bionic Leg. (**B**) Partially sectioned view of the prosthesis model highlighting the main electrical and mechanical components.
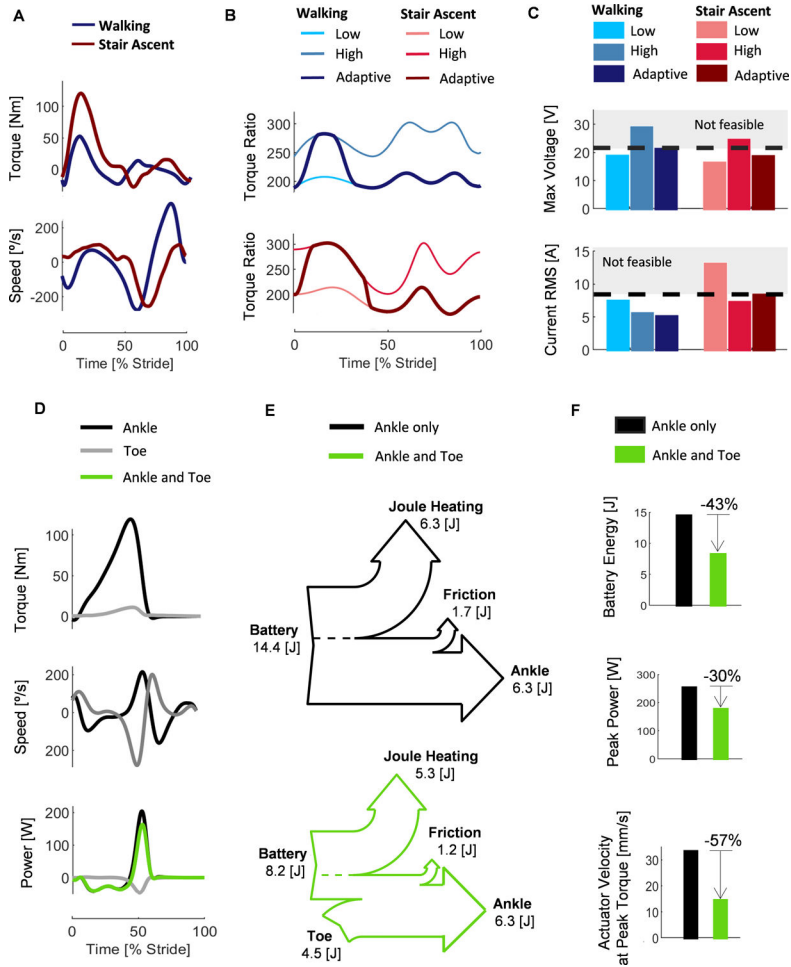
Figure 2. Analysis of the torque-sensitive actuator and the compliant underactuated mechanism.
(**A**) Biological knee torque and speed during walking and stair ascent for nonamputee individuals. (**B**) Predicted torque ratio during walking and stair ascent. (**C**) Predicted current root mean square (RMS) and maximum winding voltage for walking and stair ascent. (**D**) Torque, speed, and power of the ankle and toe during walking and stair ascent. (**E**) Predicted energy flow analysis for the underactuated ankle/toe mechanism and ankle-only design. (**F**) Predicted electrical energy, actuator peak power, and velocity at peak torque for the underactuated ankle/toe mechanism and ankle-only design.
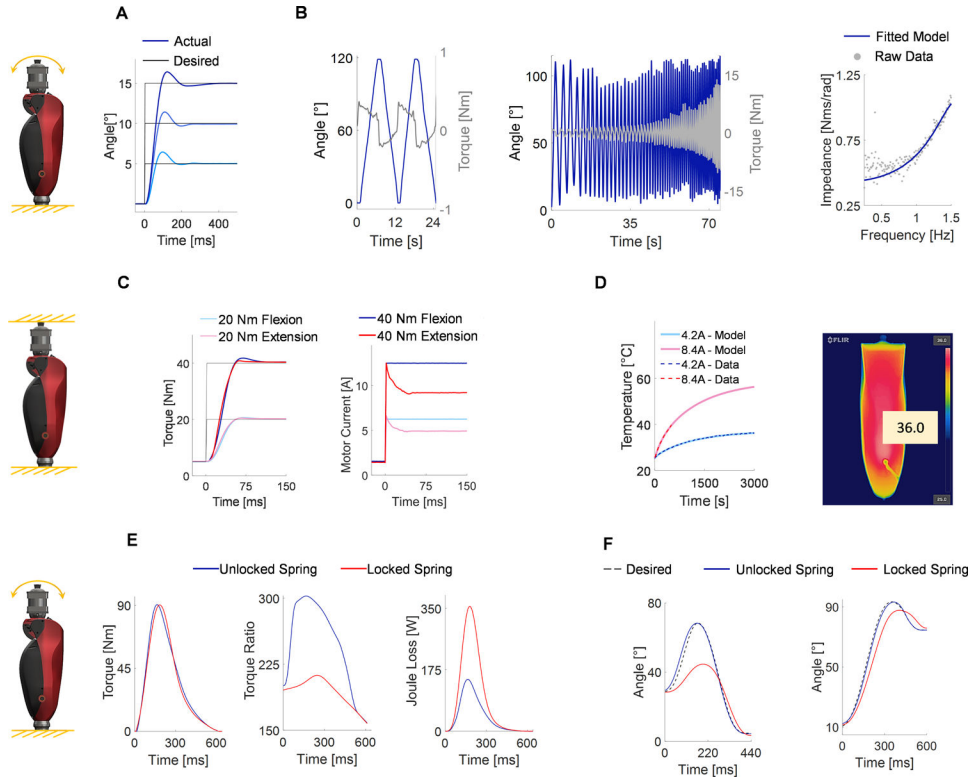
Figure 3. Characterization of the knee module on the bench.
(**A**) Step response of the knee closed-loop position controller. (**B**) Knee backdriving torque and estimated impedance. Ascent. (**C**) Knee torque step response and corresponding motor current. (**D**) Temperature of the knee motor housing/frame for different motor currents and corresponding knee frame thermal imaging. (**E**) Bell-shaped knee torque input and corresponding knee torque ratio and knee Joule heating losses. (**F**) Tracking of representative position profiles for the swing phase of walking and stair ascent.
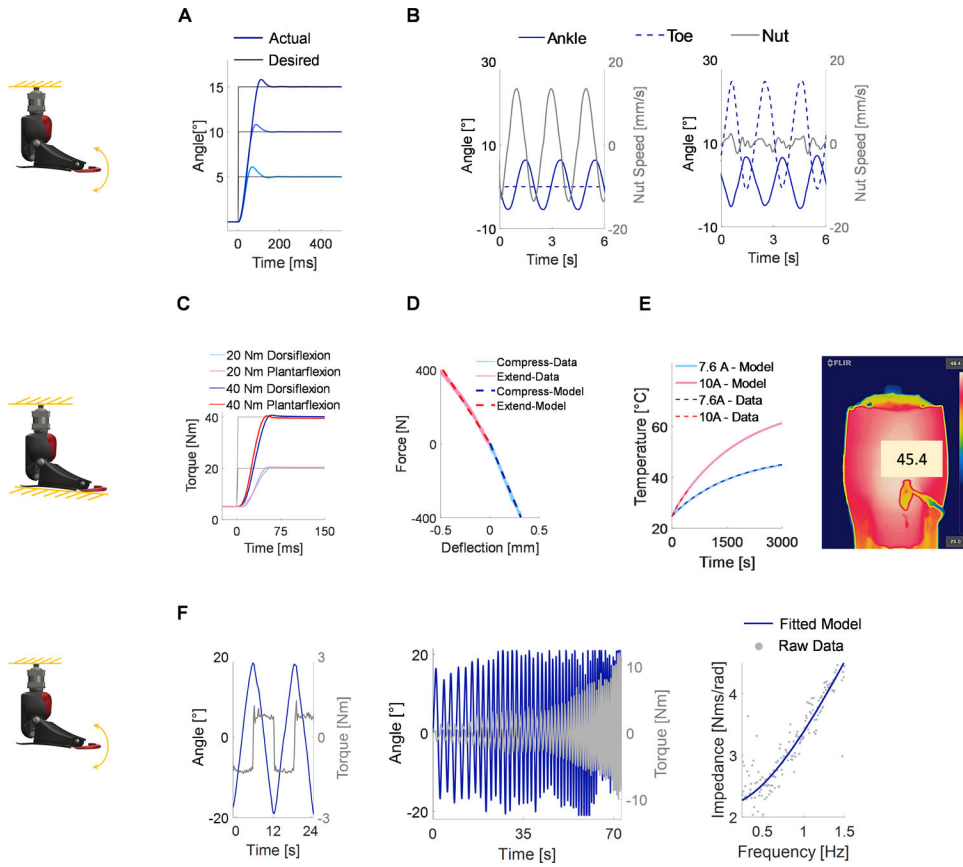
Figure 4. Characterization of the ankle module on the bench.
(**A**) Step response of the ankle closed-loop position controller. (**B**) Linear actuator speed for sinusoidal position input at the ankle and fixed toe and for sinusoidal position input at both the ankle and the toe. (**C**) Ankle torque step response. (**D**) Linear spring characterization in compression and extension. (**E**) Temperature of the ankle motor housing/frame for different motor currents and corresponding ankle frame thermal imaging. (**F**) Ankle backdriving torque and estimated impedance.

Figure 5. Above-knee amputee participants ambulating with the Utah Bionic Leg.
Representative images of the three participants ambulating on the treadmill and staircase.
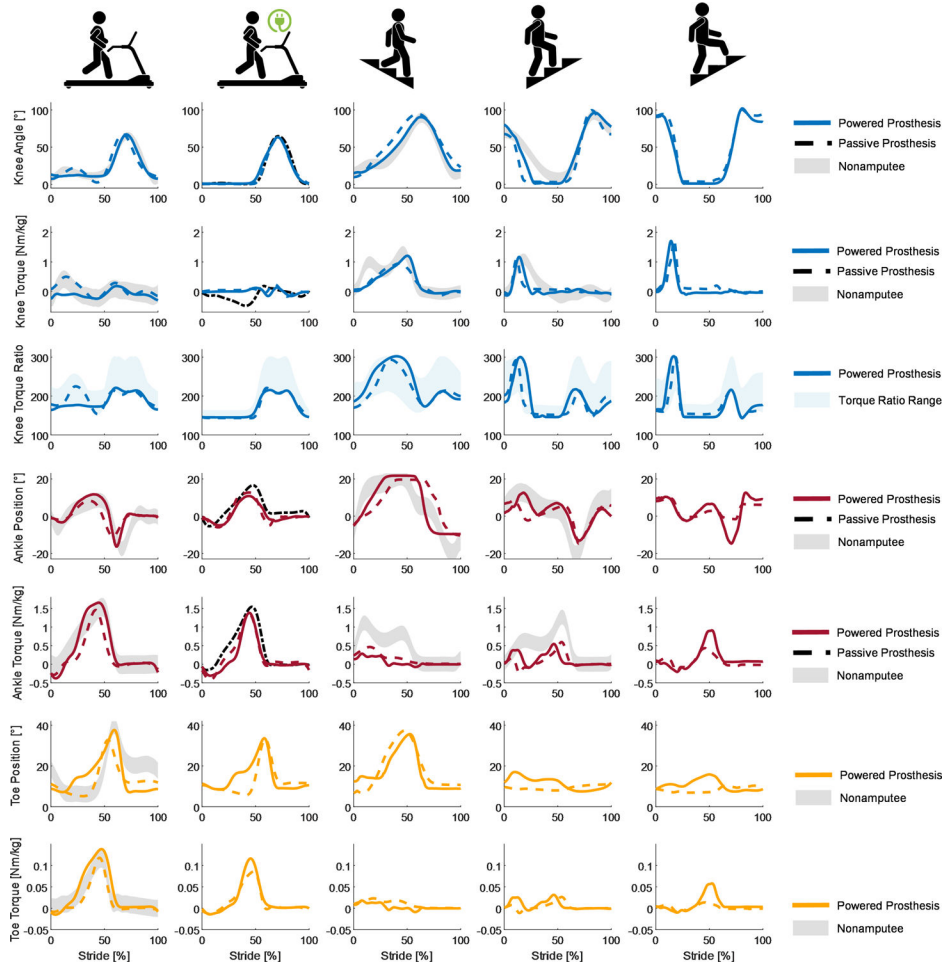
Figure 6. Kinematics and kinetics across five ambulation activities, with joint angles, joint moments and knee torque ratio recorded with three amputee participants.
Colored lines denote mean values across 10 strides. Shaded areas in grey denote nonamputee biomechanical reference, and shaded areas in purple denote passive prosthesis reference. For Knee Torque Ratio plots, shaded areas in blue denote the bounds of the torque ratio variation.
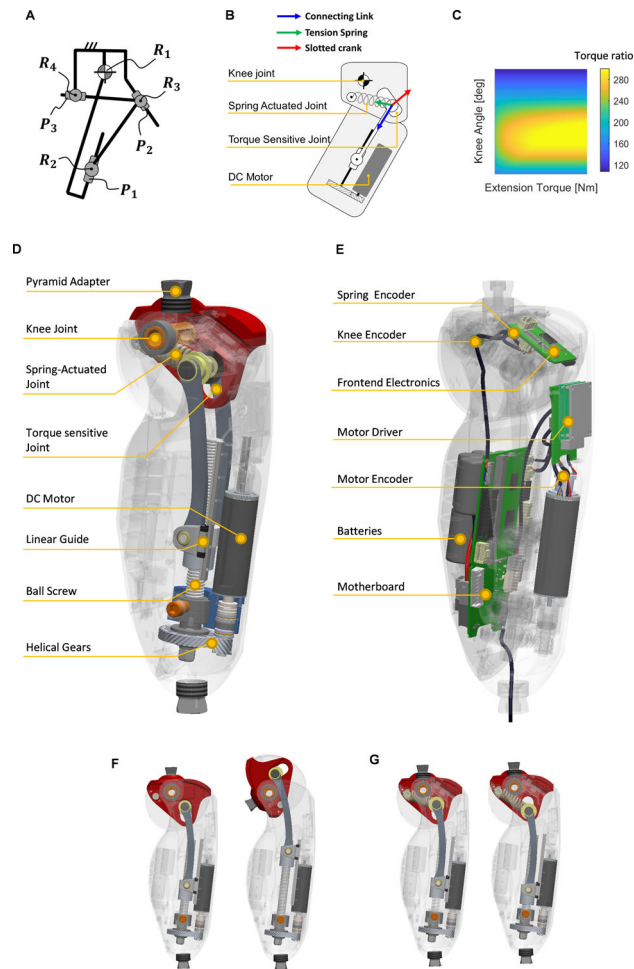
Figure 7. Knee design

(**A**) Kinematic diagram of the torque-sensitive actuator. (**B**) Schematic representation of the torque sensitive actuator highlighting the forces acting on the torque-sensitive joint. (**C**) Knee torque ratio as a function of the knee angle and the knee extension torque. (**D**) Knee model highlighting the main mechanical components. (**E**) Knee model highlighting the main electrical components. (**F**) Range of motion of the knee joint. (**G**) Range of motion of the torque-sensitive joint.
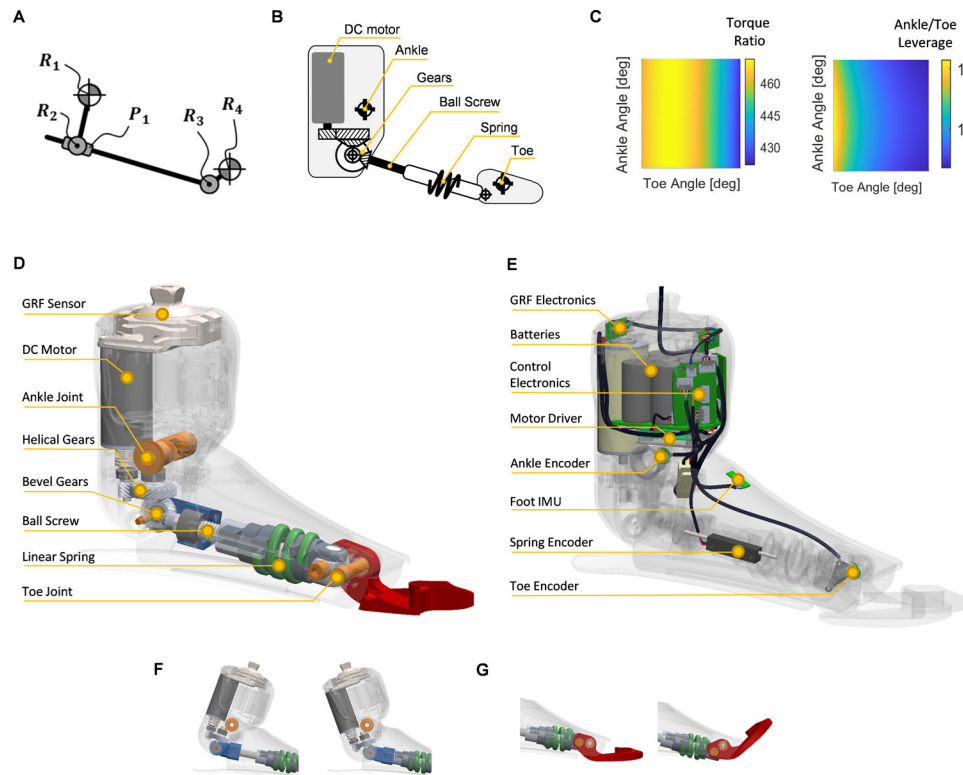
Figure 8. Ankle design.

(**A**) Kinematic diagram of the underactuated mechanism. (**B**) Schematic representation of the compliant underactuated mechanism. (**C**) Ankle torque ratio and ankle/toe leverage as a function of the ankle angle and the toe angle. (**D**) Ankle model highlighting the main mechanical components. (**E**) Ankle model highlighting the main electrical components. (**F**) Range of motion of the ankle joint. (**G**) Range of motion of the toe joint.

Table 1

Clinically Relevant Goal and Metrics

Goal	Metric	Walking	Stair Ascent	Stair Descent
Controlled weight acceptance	Knee angle at heel strike (°)	9.3 (7.0)[*]	71.8 (69.1)	15.4 (16.6)
	Ankle early stance PF (°)	2.8 (3.8)	8.1 (12.7)	NA
	Maximum Stance Knee Flexion (°)	13.7 (19.2)	NA	NA
Ambulation at Desired Speed	Ankle Pushoff Time (%)	60.9 (66.0)	72.5 (67.0)	NA
	Knee Swing Extension Time (%)	70.7 (72.3)	82.4 (83.8)	62.4(63.9)
Appropriate Torque for Support and Propulsion	Knee Maximum Extension Torque in Stance (Nm/kg)	0.33 (0.4)	1.08 (1.09)	1.05 (1.34)
	Ankle Pushoff Torque (Nm/kg)	1.50 (1.53)	0.62 (1.26)	NA
Appropriate amount of swing clearance	Knee swing flexion (°)	65.5 (65.5)	99.9 (93.7)	93.4(89.4)
	Ankle swing movement (°)	14.2 (17.5)	16.1 (29.7)	9.9 (22.9)
Reciprocal Gait Pattern	Visual Inspection	NA	Yes	Yes
Foot Mechanics	Toe Maximum Extension (°)	36.3 (39.6)	12.5	36.0
	Toe Maximum Torque (Nm/kg)	0.12 (0.12)	0.03	0.03

[*] Numbers in parentheses are derived from nonamputee reference